PROCEEDINGS OF SCIENCE

Update on $B \to D^* \ell \nu$ form factor at zero-recoil using the Oktay-Kronfeld action

Tanmoy Bhattacharya, Rajan Gupta, Sungwoo Park*
Theoretical Division T-2, Los Alamos National Laboratory, Los Alamos, NM 87545, USA
E-mail: tanmoy@lanl.gov, rg@lanl.gov, sungwoo@lanl.gov

Yong-Chull Jang
Phsics Department, Brookhaven National Laboratory, Upton, NY 11973, USA
E-mail: ypj@bnl.gov

Jon A. Bailey, Benjamin J. Choi, Hwancheol Jeong, Seungyeob Jwa, Sunkyu Lee, Weonjong Lee, Jeonghwan Pak
Lattice Gauge Theory Research Center, CTP, and FPRD,
Department of Physics and Astronomy, Seoul National University, Seoul 08826, South Korea
E-mail: jabsnu@gmail.com, wlee@snu.ac.kr

Jaehoon Leem
School of Physics, Korea Institute for Advanced Study (KIAS), Seoul 02455, South Korea
E-mail: leemjaehoon@kias.re.kr

LANL/SWME Collaboration

We present an update on the calculation of $\bar{B} \to D^* \ell \bar{\nu}$ semileptonic form factor at zero recoil using the Oktay-Kronfeld bottom and charm quarks on $N_f = 2+1+1$ flavor HISQ ensembles generated by the MILC collaboration. Preliminary results are given for two ensembles with $a \approx 0.12$ and 0.09 fm and $M_\pi \approx 310$ MeV. Calculations have been done with a number of valence quark masses, and the dependence of the form factor on them is investigated on the $a \approx 0.12$ fm ensemble. The excited state is controlled by using multistate fits to the three-point correlators measured at 4–6 source-sink separations.

The 36th Annual International Symposium on Lattice Field Theory - LATTICE2018
22-28 July, 2018
Michigan State University, East Lansing, Michigan, USA.

*Speaker.

PoS(LATTICE2018)283

1. Introduction

Lattice calculation of $\bar{B} \to D^* \ell \bar{\nu}$ semileptonic decay form factors can be used to determine the CKM matrix element $|V_{cb}|$ from the measured exclusive decay rates. Precise results for exclusive $|V_{cb}|$ will address the well-known $\approx 3\sigma$ discrepancy from the inclusive determination of $|V_{cb}|$ [1]. In addition, there is an analysis showing $\approx 4\sigma$ tension in the standard model evaluation of $|\varepsilon_K|$ [2] using the exclusive $|V_{cb}|$.

For the $\bar{B} \to D^* \ell \bar{\nu}$ study, the heavy quark discretization error, estimated by HQET power counting in terms of $\lambda_c \sim \dfrac{\Lambda_{QCD}}{2m_c} \sim \dfrac{500\text{ MeV}}{2 \times 1.3\text{ GeV}} \sim \dfrac{1}{5}$, is dominant especially for charm. Calculations of the zero recoil form factor $\mathscr{F}(w=1) = h_{A_1}(1)$ using the Fermilab action has $\mathscr{O}(\lambda_c^3) \sim 1\%$ uncertainty assuming $\alpha_s \sim \lambda_c$. To achieve precision below 1% in $|V_{cb}|$, we propose to use the Oktay-Kronfeld (OK) action, in which the discretization error are $\mathscr{O}(\lambda_c^4) \sim 0.2\%$ provided a full one-loop improvement of correction terms is carried out [3, 4]. In this work, we are working with tree-level tadpole-improvement of the action and current operators since the one-loop calculations are not complete.

We calculate the form factor $h_{A_1}(1)$ using the double ratio of ground state matrix elements [5],

$$|h_{A_1}(1)|^2 = \frac{\langle D^*|A^j_{cb}|\bar{B}\rangle \langle \bar{B}|A^j_{bc}|D^*\rangle}{\langle D^*|V^4_{cc}|D^*\rangle \langle \bar{B}|V^4_{bb}|\bar{B}\rangle} \times \rho^2_{A_j}, \quad \text{with} \quad \rho^2_{A_j} = \frac{Z^{cb}_{A_j} Z^{bc}_{A_j}}{Z^{cc}_{V_4} Z^{bb}_{V_4}}. \tag{1.1}$$

$\rho^2_{A_j}$ is the matching factor that is expected to be close to unity [5]. Each of the matrix element is extracted from the related three-point function calculated on the lattice. For example, $\langle D^*|A^j_{cb}|B\rangle$ is from $C^{B\to D^*}_{A_1}(t,\tau)$ defined in Eq. (2.2). We also use an improved current operator $A^{cb}_j(y) = \bar{\Psi}_c(y)\gamma_j\gamma_5\Psi_b(y)$ where the improved field $\Psi(x)$ is obtained by the following field rotation on the unimproved fermion field $\psi(x)$: $\Psi(x) = [1 + \sum_i d_i \mathscr{R}_i]\psi(x)$. Improvement up to $\mathscr{O}(\lambda^3)$ can be obtained using tree-level matching of the coefficients d_i and operators $\mathscr{R}_i$ [6, 7].

We present an update on our previous calculation of $|h_{A_1}(1)/\rho_{A_j}|$ [8], paying attention to controlling the excited-state contamination (ESC) using multistate fits to 3-point (3pt) data with 4–6 source-sink time separations. The parameters in the calculation on the two $N_f = 2+1+1$ HISQ ensembles, generated by the MILC collaboration [9], are given in Table 1. The light quark propagators (u,d,s) are calculated using the HISQ action with point source and sink. For the heavy quark (c,b) propagators, we use the OK action with covariant Gaussian smearing at both the source and the sink. The hopping parameters κ_{crit}, κ_b, κ_c have been tuned nonperturbatively as described in Ref. [8].

2. Controlling excited-state contamination

To achieve sub-percent precision, we have to control the ESC. On a lattice with time extent T, the B- and D^*-meson 2-point (2pt) functions, $C^{2\text{pt}}(t)$, are fit using a $3+2$-state ansatz:

$$\begin{aligned} C^{2\text{pt}}(t) = \langle O^\dagger(t) O(0)\rangle = |\mathscr{A}_0|^2 e^{-M_0 t}\Bigg(1 &+ \left|\frac{\mathscr{A}_2}{\mathscr{A}_0}\right|^2 e^{-\Delta M_2 t} + \left|\frac{\mathscr{A}_4}{\mathscr{A}_0}\right|^2 e^{-(\Delta M_2+\Delta M_4)t} + \cdots \\ &- (-1)^t \left|\frac{\mathscr{A}_1}{\mathscr{A}_0}\right|^2 e^{-\Delta M_1 t} - (-1)^t \left|\frac{\mathscr{A}_3}{\mathscr{A}_0}\right|^2 e^{-(\Delta M_1+\Delta M_3)t} + \cdots \Bigg) + (t \leftrightarrow T-t). \end{aligned} \tag{2.1}$$

ID	a	M_π	m_x/m_s	$\kappa_{\rm crit}$	κ_c	κ_b	$\{\sigma, N_{\rm cvg}\}$	$N_{\rm cfg} \times N_{\rm src}$	τ
$a12m310$	0.1207	305	0.1, 0.2†, 0.3, 0.4, 1.0	0.051211	0.048524	0.04102	$\{1.5, 5\}$	1053×3	10, 11, 12, 13, 14, 15
$a09m310$	0.0888	313	0.2†, 1.0	0.05075	0.04894	0.0429	$\{2, 10\}$	1001×3	15, 16, 17, 18

Table 1: Parameters used in the measurements performed on two MILC HISQ gauge ensembles described in Ref. [9]. m_x/m_s is the ratio of valence spectator quark mass to the sea strange quark mass where † denotes the unitary point for the degenerate up and down quarks. Hopping parameters $\kappa_{\rm crit}$, κ_c and κ_b give the values obtained for the critical and the charm and the bottom quark masses. $\{\sigma, N_{\rm cvg}\}$ are parameters for the covariant Gaussian smearing. $N_{\rm cfg} \times N_{\rm src}$ denotes the number of measurements made. τ gives the source-sink time separations simulated.

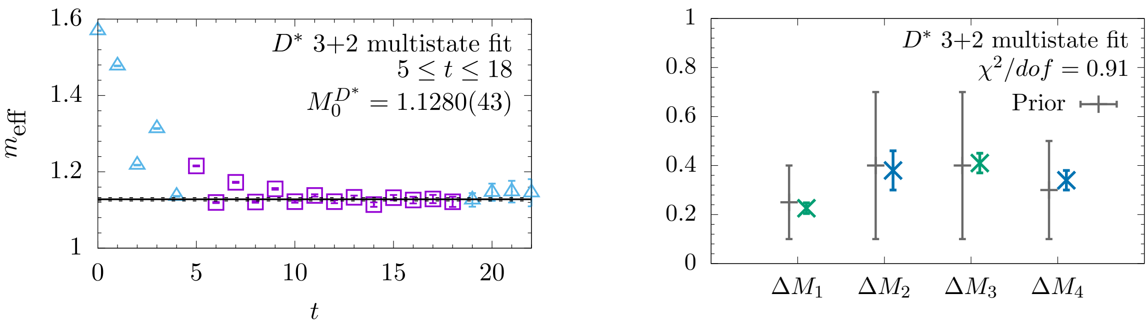

Figure 1: (Left) Effective mass, $m_{\rm eff}(t) \equiv \frac{1}{2}\ln|C^{2pt}(t)/C^{2pt}(t+2)|$, plot using the 3+2-state fit to the 2pt function on the a12m310 ensemble for the D^*-meson with $m_x/m_s = 0.2$. The ground state mass is shown as a horizontal line. (Right) The excited state masses from the 3+2-states fit using empirical Bayesian priors.

where O is the meson interpolating operator. $\Delta M_n \equiv M_n - M_{n-2}$ with $n = 2, 4$ are the mass gaps for even parity, and $\Delta M_1 \equiv M_1 - M_0$ and $\Delta M_3 \equiv M_3 - M_1$ for the two odd parity states that arise in staggered formulations. An empirical Bayesian method is used to fix the priors for the excited-state masses M_n and amplitudes $\mathscr{A}_n = \langle n|O|\Omega\rangle$ to stabilize the fits as described in Ref. [10]. Fig. 1 illustrates the results for the ground- and excited-state masses of D^* meson and the priors used for excited states.

The 3pt data is fit including $2+1$ states for $|B_m\rangle$ and $|D_n^*\rangle$ in the spectral decomposition:

$$C_{A_j}^{B\to D^*}(t,\tau) = \langle O_{D^*}^\dagger(0) A_j^{cb}(t) O_B(\tau)\rangle \qquad (0 < t < \tau) \tag{2.2}$$

$$\begin{aligned}
&= \mathscr{A}_0^{D^*}\mathscr{A}_0^{B}\langle D_0^*|A_j^{cb}|B_0\rangle e^{-M_{B_0}(\tau-t)}e^{-M_{D_0^*}t} - \mathscr{A}_0^{D^*}\mathscr{A}_1^{B}\langle D_0^*|A_j^{cb}|B_1\rangle(-1)^{\tau-t}e^{-M_{B_1}(\tau-t)}e^{-M_{D_0^*}t} \\
&\quad - \mathscr{A}_1^{D^*}\mathscr{A}_0^{B}\langle D_1^*|A_j^{cb}|B_0\rangle(-1)^{t}e^{-M_{B_0}(\tau-t)}e^{-M_{D_1^*}t} + \mathscr{A}_1^{D^*}\mathscr{A}_1^{B}\langle D_1^*|A_j^{cb}|B_1\rangle(-1)^{\tau}e^{-M_{B_1}(\tau-t)}e^{-M_{D_1^*}t} \\
&\quad + \mathscr{A}_2^{D^*}\mathscr{A}_0^{B}\langle D_2^*|A_j^{cb}|B_0\rangle e^{-M_{B_0}(\tau-t)}e^{-M_{D_2^*}t} + \mathscr{A}_0^{D^*}\mathscr{A}_2^{B}\langle D_0^*|A_j^{cb}|B_2\rangle e^{-M_{B_2}(\tau-t)}e^{-M_{D_0^*}t} \\
&\quad - \mathscr{A}_2^{D^*}\mathscr{A}_1^{B}\langle D_2^*|A_j^{cb}|B_1\rangle(-1)^{\tau-t}e^{-M_{B_1}(\tau-t)}e^{-M_{D_2^*}t} - \mathscr{A}_1^{D^*}\mathscr{A}_2^{B}\langle D_1^*|A_j^{cb}|B_2\rangle(-1)^{t}e^{-M_{B_2}(\tau-t)}e^{-M_{D_1^*}t} \\
&\quad + \mathscr{A}_2^{D^*}\mathscr{A}_2^{B}\langle D_2^*|A_j^{cb}|B_2\rangle e^{-M_{B_2}(\tau-t)}e^{-M_{D_2^*}t} + \cdots,
\end{aligned} \tag{2.3}$$

where A_j^{cb} is the improved axial current inserted at time t, and $\mathscr{A}_n^B$, $\mathscr{A}_m^{D^*}$, $M_{D_n^*}$ and M_{B_m} values are taken from fits to the 2pt functions. Similar fit functions are used for the other channels: $C_{A_1}^{D^*\to B}(t,\tau)$, $C_{V_4}^{B\to B}(t,\tau)$ and $C_{V_4}^{D^*\to D^*}(t,\tau)$. In all the fits, we skip four points next to the source and

Current	$\langle B\|V_4\|B\rangle$	χ^2/dof [p]	$\langle D^*\|V_4\|D^*\rangle$	χ^2/dof [p]	$\langle D^*\|A_j\|B\rangle$	χ^2/dof [p]	$\langle B\|A_j\|D^*\rangle$	χ^2/dof [p]
Unimp.	3.88(8)	1.20 [0.21]	8.44(17)	0.73 [0.84]	4.79(10)	0.73 [0.84]	4.84(11)	0.89 [0.63]
$\mathcal{O}(\lambda)$	3.89(8)	1.20 [0.21]	8.45(17)	0.73 [0.84]	4.90(10)	0.74 [0.83]	4.96(12)	0.84 [0.70]
$\mathcal{O}(\lambda^2)$	3.74(8)	1.27 [0.15]	7.50(15)	0.86 [0.68]	4.71(10)	0.73 [0.84]	4.79(11)	0.93 [0.56]

(a) Results for the $a12m310$ ensemble with $m_x = 0.2m_s$.

Current	$\langle B\|V_4\|B\rangle$	χ^2/dof [p]	$\langle D^*\|V_4\|D^*\rangle$	χ^2/dof [p]	$\langle D^*\|A_j\|B\rangle$	χ^2/dof [p]	$\langle B\|A_j\|D^*\rangle$	χ^2/dof [p]
Unimp.	4.64(12)	1.44 [0.05]	9.26(22)	0.90 [0.63]	5.49(10)	1.54 [0.03]	5.48(15)	0.68 [0.91]
$\mathcal{O}(\lambda)$	4.65(12)	1.44 [0.05]	9.27(22)	0.90 [0.63]	5.60(10)	1.54 [0.03]	5.60(15)	0.67 [0.92]
$\mathcal{O}(\lambda^2)$	4.42(12)	1.34 [0.09]	8.10(19)	0.84 [0.73]	5.33(10)	1.62 [0.02]	5.32(15)	0.76 [0.83]

(b) Results for the $a09m310$ ensemble with $m_x = 0.2m_s$.

Table 2: Matrix elements of $\mathcal{O}(\lambda^\ell)$ (with $\ell \in 0,1,2$) improved currents extracted from $2+1$-state fits.

the sink that have the largest ESC. In Fig. 2, we display the ratio, $\mathcal{G}$,

$$\mathcal{G}(t,\tau) \equiv \frac{C_{A_j}^{B\to D^*}(t,\tau)}{\mathcal{A}_0^{D^*}\mathcal{A}_0^{B} e^{-M_{B_0}(\tau-t)} e^{-M_{D_0^*}t}} = \langle D_0^*|A_j^{cb}|B_0\rangle + \cdots , \tag{2.4}$$

where $\mathcal{A}_0^B$, $\mathcal{A}_0^{D^*}$, $M_{D_0^*}$ and M_{B_0} are ground-state amplitudes and masses determined from 2pt function fits. $\mathcal{G}$ asymptotes to the ground state matrix element in the $t \to \infty$ and $\tau - t \to \infty$ limits. The data show the size of the ESC and the oscillatory nature of the convergence. The $(-1)^\tau \langle D_1^*|A_j^{cb}|B_1\rangle$ term controls the even-odd oscillation about the grey band while $\langle D_2^*|A_j^{cb}|B_2\rangle$ controls the convergence as $\tau \to \infty$ for both even or odd τ data. We also find that the contribution of terms of the form $(-1)^{\tau-t}\langle D_0^*|A_j^{cb}|B_1\rangle$ is tiny and that of $(-1)^{\tau-t}\langle D_1^*|A_j^{cb}|B_2\rangle$ is negligible. The latter is therefore set to zero in the final fits. On the other hand, the grey horizontal band in Fig. 2 is the ground-state matrix element obtained by fitting $C_{A_j}^{B\to D^*}(t,\tau)$ using Eq. (2.3), to which $\mathcal{G}$ should converge. These results from the fits are summarized in Table 2. Note that there is no significant improvement at $\mathcal{O}(\lambda)$ in $\langle B|V_4|B\rangle$ and $\langle D^*|V_4|D^*\rangle$, but a large change at $\mathcal{O}(\lambda^2)$ [1] (also see Fig. 4). Thus, higher order improvements for these two channels may be necessary.

3. $|h_{A_1}(1)/\rho_{A_j}|$ result

We obtain $|h_{A_1}(1)/\rho_{A_j}|^2$, defined in Eq. (1.1), using the ground-state matrix elements given in Table 2. The result for the two values of the lattice spacing at fixed pion mass $M_\pi \approx 310$ MeV (unitary point) is shown by the grey horizontal band in all panels of Fig. 3. The error estimate includes the uncertainty coming from the fits used to remove excited-state effects. The left two panels in Fig. 3 show the data for the double ratio $R(t,\tau)$

$$R(t,\tau) = \frac{C_{A_1}^{B\to D^*}(t,\tau)C_{A_1}^{D^*\to B}(t,\tau)}{C_{V_4}^{B\to B}(t,\tau)C_{V_4}^{D^*\to D^*}(t,\tau)}, \tag{3.1}$$

that significantly cancels the ESC in each individual correlator illustrated in Fig. 2. The right panels in Fig. 3 show the linear combination $\overline{R}(t,\tau)$ defined as [5],

$$\overline{R}(t,\tau) = \frac{1}{2}R(t,\tau) + \frac{1}{4}R(t,\tau+1) + \frac{1}{4}R(t+1,\tau+1), \tag{3.2}$$

[1] Here, we used the $\mathcal{O}(\lambda^2)$ improvement coefficient for the current given in the Ref. [6]. Taking the coefficient from Ref. [7] results in a negligible change. Full $\mathcal{O}(\lambda^3)$ current improvement presented in Ref. [7] is being implemented.

PoS(LATTICE2018)283

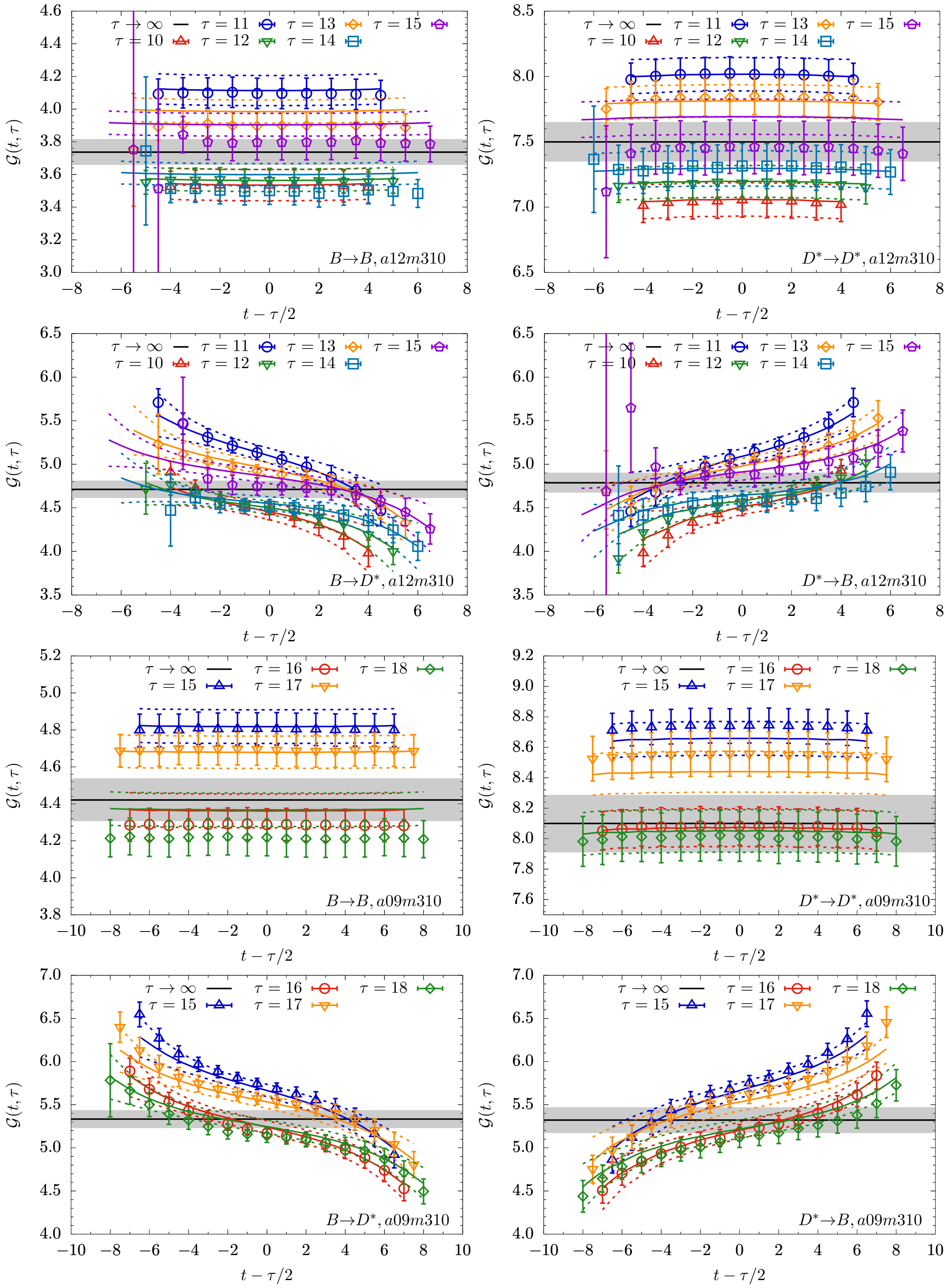

Figure 2: Data for the ratio $\mathcal{G}$ for the various values of τ (see labels) are plotted versus $t - \tau/2$ for the $\mathcal{O}(\lambda^2)$ improved current and $m_x = 0.2 m_s$. The horizontal line is the ground-state matrix element ($\tau \to \infty$) determined from the multistate fit using Eq. (2.3). The results of the fit for each τ is shown in the same color as the data. Note the difference in ESC for $D^* \to B$ (or the rough mirror process $B \to D^*$) and $D^* \to D^*$ (or $B \to B$) and the change with a between $a12m310$ (top 4 panels) and $a09m310$ (bottom 4 panels).

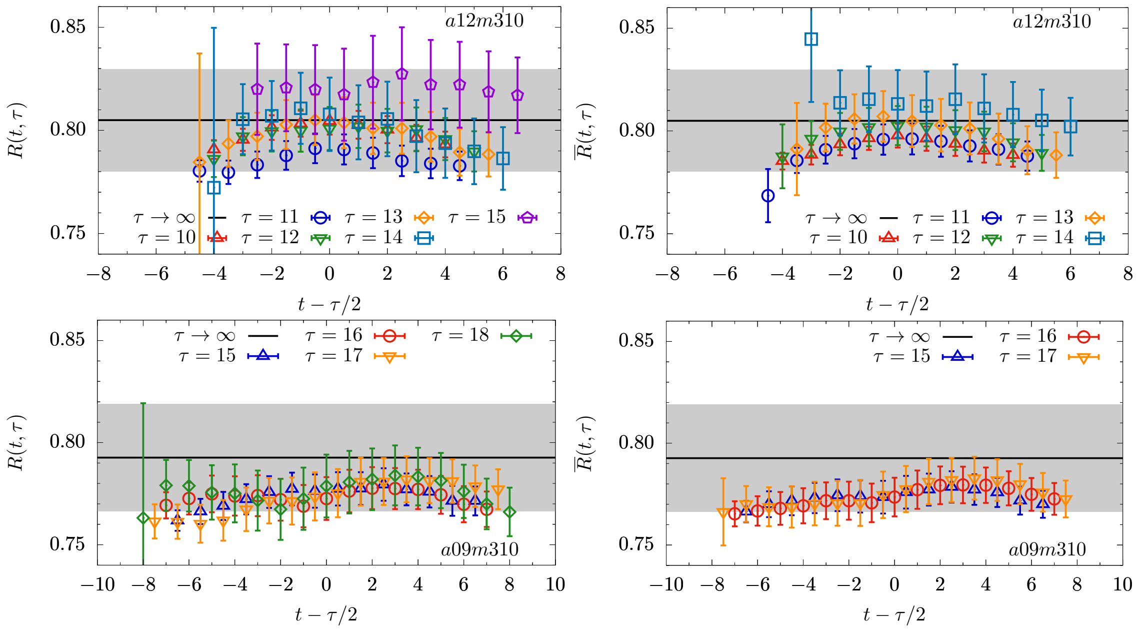

Figure 3: Data for the double ratio $R(t, \tau)$ for the various values of τ are plotted versus the operator insertion time $t - \tau/2$. The grey horizontal band is the result for $|h_{A_1}(1)/\rho_{A_j}|^2$ obtained using Eq. (1.1). The top (bottom) panels show data for the $a12m310$ ($a09m310$) ensemble at the unitary point $m_x = 0.2 m_s$. The left (right) panels show data for $R(t, \tau)$ ($\overline{R}(t, \tau)$) that are defined in the text.

that further suppresses the ESC, especially from the opposite parity states. Since the grey band in Fig. 3 is constructed as the ratio of ground state matrix elements (albeit evaluated using 2+1 state fits), both the ratios, $R(t, \tau)$ and $\overline{R}(t, \tau)$ should asymptote to it in the $t \to \infty$ and $(\tau - t) \to \infty$ limits. We find that $R(t, \tau)$ and $\overline{R}(t, \tau)$ overlap with the grey band, however the spread due to remaining ESC is larger in $R(t, \tau)$ than in $\overline{R}(t, \tau)$. In fact, on the finer $a09m310$ ensemble, we do not observe a spread in $\overline{R}(t, \tau)$ versus τ, however, the comparison with the grey band suggests that quoting the average of the $\overline{R}(t, \tau)$ data as the final result could underestimate the error.

The data for $|h_{A_1}(1)/\rho_{A_j}|$ in Fig. 4 (left) show no significant dependence on the spectator quark mass m_x. The observed dependence on the order of improvement in the current is unexpected from naive HQET power counting and could an artifact of setting $\rho_{A_j} = 1$, which also depends on the order of improvement. In Fig. 4 (right), we compare our results with those from the FNAL/MILC and HPQCD collaborations [5, 11] obtained in the continuum limit. The $O(\lambda^2)$ data are consistent with the FNAL/MILC and HPQCD results and show no significant lattice spacing dependence. This rough agreement provides a good and encouraging check of our calculations that are being done with a much more complicated heavy quark action and current.

A brief summary of the work under progress is as follows. (i) Analysis with the $\mathscr{O}(\lambda^3)$-improvement terms in the current, (ii) analysis of the data for the nonzero recoil form factors in $B \to D^{(*)} \ell \nu$ decays, and (iii) the analysis for the decay constants f_D, f_{D_s}, f_B, f_{B_s} and f_{B_c}.

Acknowledgments

We thank the MILC collaboration for sharing the $2+1+1$-flavor HISQ ensembles generated by them. Computations for this work were carried out in part on (i) facilities of the USQCD

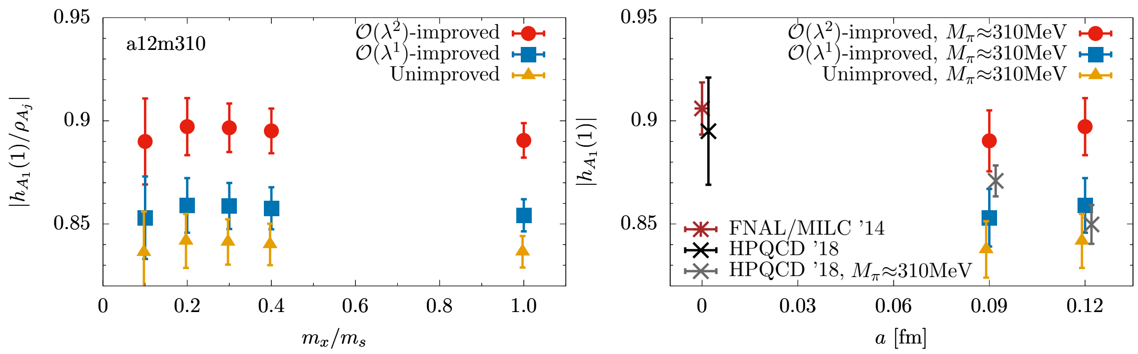

Figure 4: (Left) Data for $|h_{A_1}(1)/\rho_{A_1}|$ for three levels of current improvement plotted versus the spectator quark mass m_x for the $a12m310$ ensemble. (Right) Comparison of data on two different ensembles, $a12m310$ and $a09m310$ at the unitary point $m_x = 0.2m_s$, and with $\rho_{A_1} = 1$ to investigate a dependence, and to compare with FNAL/MILC and HPQCD collaboration results [5, 11] obtained in the continuum limit.

collaboration, which are funded by the Office of Science of the U.S. Department of Energy, and (ii) the DAVID GPU clusters at Seoul National University. The research of W. Lee is supported by the Creative Research Initiatives Program (No. 2017013332) of the NRF grant funded by the Korean government (MEST). W. Lee acknowledges support from the KISTI supercomputing center through the strategic support program for the supercomputing application research (No. KSC-2016-C3-0072).

References

[1] Y. Amhis *et al. Eur. Phys. J.* **C77** (2017), no. 12 895, [1612.07233].

[2] J. A. Bailey, S. Lee, W. Lee, J. Leem, and S. Park 1808.09657.

[3] M. B. Oktay and A. S. Kronfeld *Phys. Rev.* **D78** (2008) 014504, [0803.0523].

[4] J. A. Bailey, C. DeTar, Y.-C. Jang, A. S. Kronfeld, W. Lee, and M. B. Oktay *Eur. Phys. J.* **C77** (2017), no. 11 768, [1701.00345].

[5] J. A. Bailey *et al. Phys. Rev.* **D89** (2014), no. 11 114504, [1403.0635].

[6] A. X. El-Khadra, A. S. Kronfeld, and P. B. Mackenzie *Phys. Rev.* **D55** (1997) 3933–3957, [hep-lat/9604004].

[7] J. Bailey, Y.-C. Jang, W. Lee, and J. Leem *EPJ Web Conf.* **175** (2018) 14010, [1711.01777].

[8] J. A. Bailey, T. Bhattacharya, R. Gupta, Y.-C. Jang, W. Lee, J. Leem, S. Park, and B. Yoon *EPJ Web Conf.* **175** (2018) 13012, [1711.01786].

[9] A. Bazavov *et al. Phys. Rev.* **D87** (2013), no. 5 054505, [1212.4768].

[10] B. Yoon *et al. Phys. Rev.* **D95** (2017), no. 7 074508, [1611.07452].

[11] J. Harrison, C. Davies, and M. Wingate *Phys. Rev.* **D97** (2018), no. 5 054502, [1711.11013].